Electronic Supplementary Material (ESI) for Nanoscale.
This journal is © The Royal Society of Chemistry 2016

Electronic Supplementary Information

for

Physically-synthesized Gold Nanoparticles Containing Multiple Nanopores for Enhanced Photothermal Conversion and Photoacoustic Imaging

1. Experimental Section

Synthesis of Porous Gold Nanoparticles: To prepare the polymer pores, three separate polymer layers were spin coated on a 4-inch-diameter Si wafer. In order, these were 1-um-thick benzocyclobutene (BCB, Dow Chemical Company, USA), 90-nm-thick polymethylglutarimide (PMGI, MicroChem Corp., USA), and 100-nm-thick polymethylmethacrylate (PMMA, Microresist Technology GmbH, Germany). The PMMA layer was then patterned by thermal nanoimprinting at 200 °C under a pressure of 40 bar for 5 min. A 4-inch Si wafer having about 5×10^{10} Si nanopillars on its surface was used as the nanoimprint mold. The pillar diameter and height were 100 and 80 nm, respectively. The Si mold was fabricated by nanosphere lithography, as described in previous reports.[1,2] Because the throughput of the proposed physical method mainly depends on the size of the nanoimprint mold and its pattern density, a current yield of about 2×10^{10} PGNs from a single nanoimprinting is reasonable considering the loss of the nanoparticles during the synthesis. After nanoimprinting, the sample was subjected to O_2 plasma etching to remove residual PMMA. The sample was then immersed in a commercial wet chemical developer (AZ 300 MIF, AZ Electronic Materials, USA) for 3 s, to form an undercut profile in the PMGI resist, and obtain an array of polymer pores. A $(3.3\text{-nm-Au}/7.5\text{-nm-Ag})_{\times 4}$/6.8-nm-Au(bottom) multilayer was then deposited by thermal evaporation. After removal of the PMMA and PMGI layers by acetone and AZ 300 MIF, respectively, the AuAg multilayerd nanodisks were annealed at 200 °C for 1 h on a hot plate, in an open atmosphere. For dealloying of the Ag, the annealed sample was immersed in nitric acid at 0 °C for 30 min. This low-temperature dealloying process reportedly reduces the size of the nanopores.[3] The dealloyed nanoparticles were then released from the sample surface, by dissolving BCB by a commercial solution (Primary Stripper A, Dow Chemical Company, USA). The nanoparticles were then collected by centrifugation, subject to solvent exchange, and then resuspended in water. The exterior and interior microstructures of the PGNs were observed by SEM (Hitachi S-4800, Japan) and TEM (FEI F30, USA, operated at 300 kV), respectively. The elemental composition of the PGNs was analyzed by inductively-coupled plasma mass spectrometry (PerkinElmer ELAN DRC II, USA). Zeta potential of the PGNs in distilled water was evaluated with a zeta potential analyzer (Zetasizer Nano-Z, Malvern, UK).

Evaluation of Photothermal Conversion Efficiency: Aqueous solutions of PGNs and GNRs were placed in a 96-well plate, at a volume of 300 μl. The samples were then irradiated by an 808-nm-wavelength diode laser (L808P1000MM; ThorLabs, USA) from the top of the suspensions, at a density of 1.5 W cm^{-2}. The temperatures of the samples were measured using an infrared camera (FLIR T-200, USA) every 1 min for a total of 5 min.

Photoacoustic Imaging: Silicone tubes filled with aqueous suspensions of NPs were subjected to PA imaging, to compare their PA conversion efficiencies. A tunable wavelength nanosecond pulsed laser (NT242, EKSPLA, Lithuania) with a pulse width of 5 ns and repetition rate of 1 kHz at 808 nm was used to excite the NPs. The collimated laser beam was focused through an objective lens with an energy density of 3.276 mJ cm^{-2}, and scanned across the silicone tubes using a 2D galvanometer scanning mirror. A customized detection module was used to confocally align the illuminated laser beam and generated ultrasound.[4] The generated PA signal was collected by an unfocused ultrasonic transducer (V326-SU, Olympus-NDT, Japan), with a center frequency of 5 MHz and a −6 dB bandwidth of 76.2%. The collected signals were amplified with a gain of 51 dB then converted by a high-speed digitizer (ATS9350, AlazarTech, Canada) to obtain cross-sectional PA images (*x-z* plane). PA images were expressed via maximum amplitude projection, which projected the maximum signal of each A-line onto an *en-face* plane (*x-y* plane). The GNRs for the photothermal conversion and PA imaging experiments were purchased from Nanopartz (product name: AC12-25-808).

Optical Coherence Tomography Imaging: The configuration of the OCT based on the Michaelson interferometer is described in detail in a previous report.[5] A superluminescent diode (SLD) with a −3 dB bandwidth of 100 nm at the center wavelength of 849 nm (BLM2-D-840-B-I-10, Superlum, Ireland) was used as the light source in the OCT system. The light from the SLD was split into reference and sample arms in a 50:50 ratio, using a broadband 2×2 optical coupler. In the sample arm, the collimated light was incident to the sample via a 2D galvanometer scanner (GVSM002, Thorlabs) and an OCT scan lens (LSM-04-BB, Thorlabs). The light reflected from the reference and sample arms was recombined and directed to the linear-wavenumber spectrometer. The interference signals generated by the path length differences between the reference and sample arms were detected by the spectrometer at the 200 kHz A-line rate. The OCT system had an axial resolution (z-axis) of 3.8 μm in air (corresponding to 2.9 μm in water), and a lateral resolution (x- and y-axes) of 24 μm. The GNRs and GNSs for OCT imaging were purchased from Nanopartz (product name: AC12-25-850) and BBI Solutions (product name: EM.GC200), respectively.

2. Stability of Porous Gold Nanoparticles

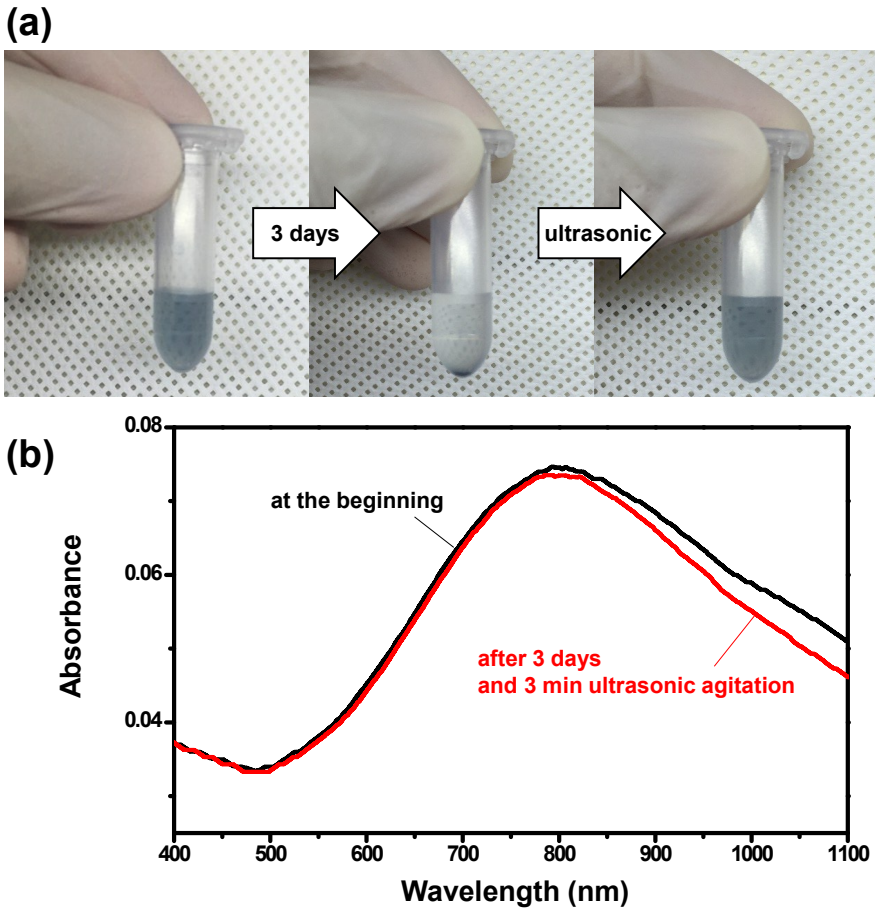

Fig. S1. (a) Photographs of aqueous solutions of the PGNs. The photographs were obtained (left) at the beginning of the test, (center) after 3 days at room temperature, and (right) after 3 days storage and 3 min ultrasonic agitation, respectively. (b) Measured absorbance curves of the 10-fold diluted aqueous solutions shown in Fig. S1a (black: absorbance of the diluted solution at the beginning, red: absorbance of the diluted solution after 3 days storage and 3 min ultrasonic agitation).

3. Non-porous Gold Nanoparticles

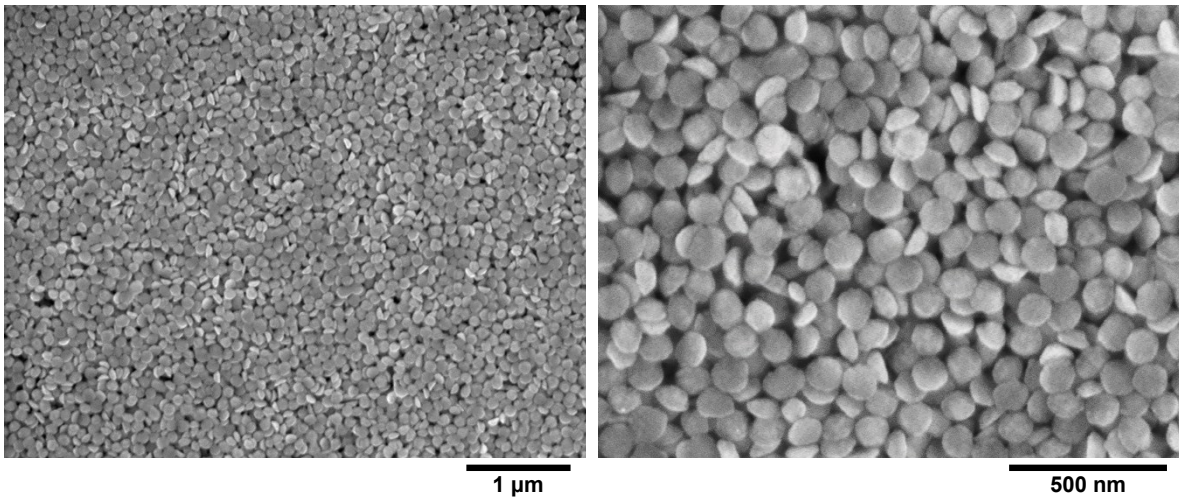

Fig. S2. SEM image of the physically synthesized non-porous gold nanoparticles.

4. Simulated Spectral Shift

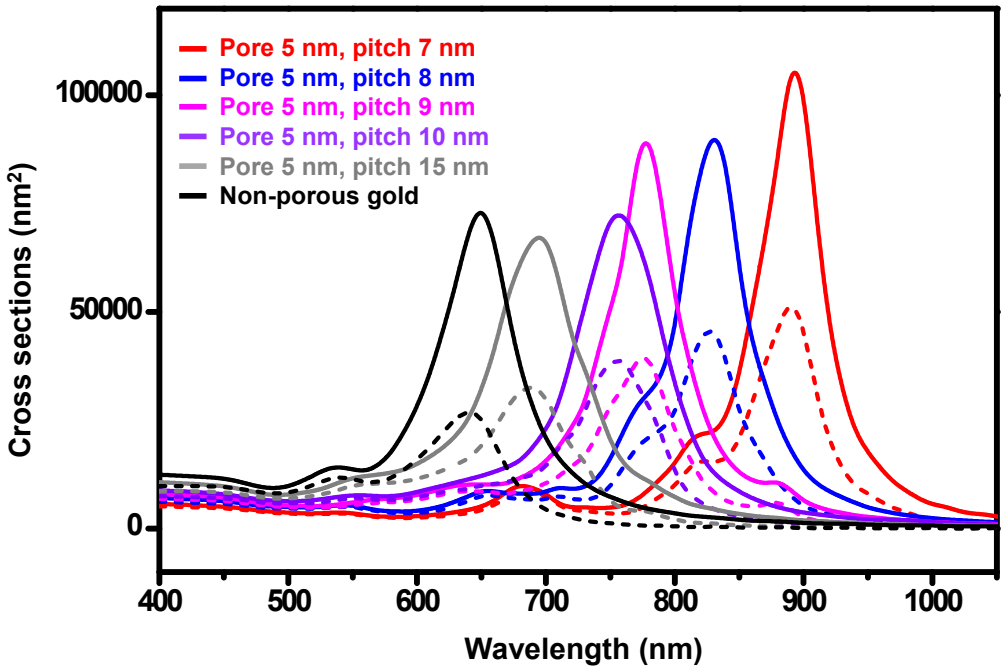

Fig. S3. Calculated extinction (solid) and absorption (dotted) cross-sections of non-porous gold nanoparticles (black) and porous gold nanoparticles with 5-nm pore diameters and pitches of 7 (red), 8 (blue), 9 (pink), 10 (violet), and 15 (gray) nm. The exterior shape and size of the gold nanoparticles were the same as those described in Figure 3c.

5. Optical properties of Commercial Gold Nanoparticles

(a)

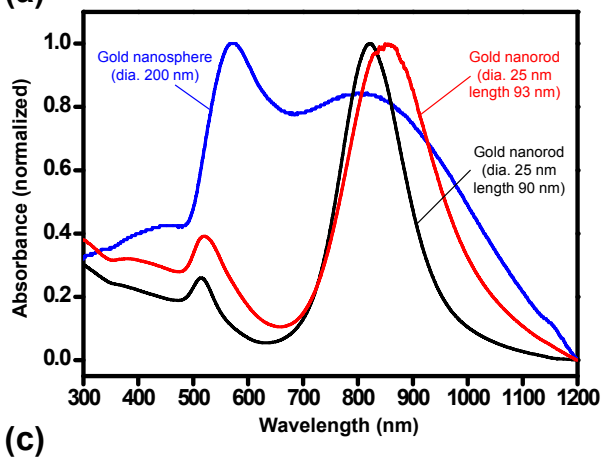

(b)

Type	Concentration	Molar extinction coefficient ($M^{-1} cm^{-1}$)
Gold nanorod (diameter 25 nm, length 90 nm)	6.5×10^{10} /ml	9.3×10^{9} (at 808 nm)
Gold nanorod (diameter 25 nm, length 93 nm)	6.2×10^{10} /ml	9.7×10^{9} (at 850 nm)
Gold nanosphere (diameter 200 nm)	7.0×10^{8} /ml	7.0×10^{11} (at 850 nm)

(c)

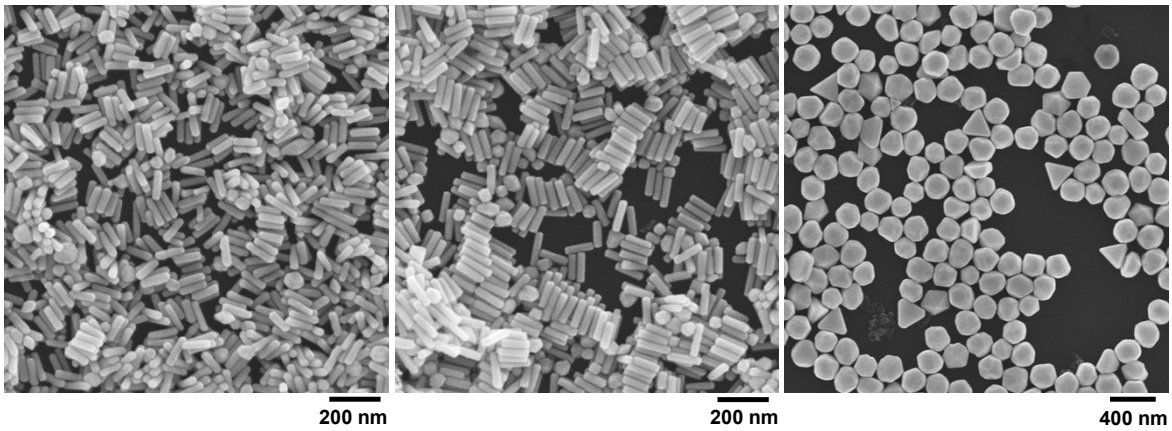

Fig. S4. (a) Measured absorbance curves of aqueous solutions of commercial GNRs (black: diameter 25 nm, length 90 nm, red: diameter 25 nm, length 93 nm) and GNSs (blue: diameter 200 nm). The GNRs and GNSs were purchased from Nanopartz (product name: AC12-25-808, AC12-25-850) and BBI Solutions (product name: EM.GC200), respectively. (b) Table of the molar extinction coefficients of the GNRs and the GNS in Fig. S4(a). The molar concentrations were given by the suppliers.[6,7] (c) SEM images of the GNRs (left: AC12-25-808, center: AC12-25-850) and the GNSs (right: EM.GC200).

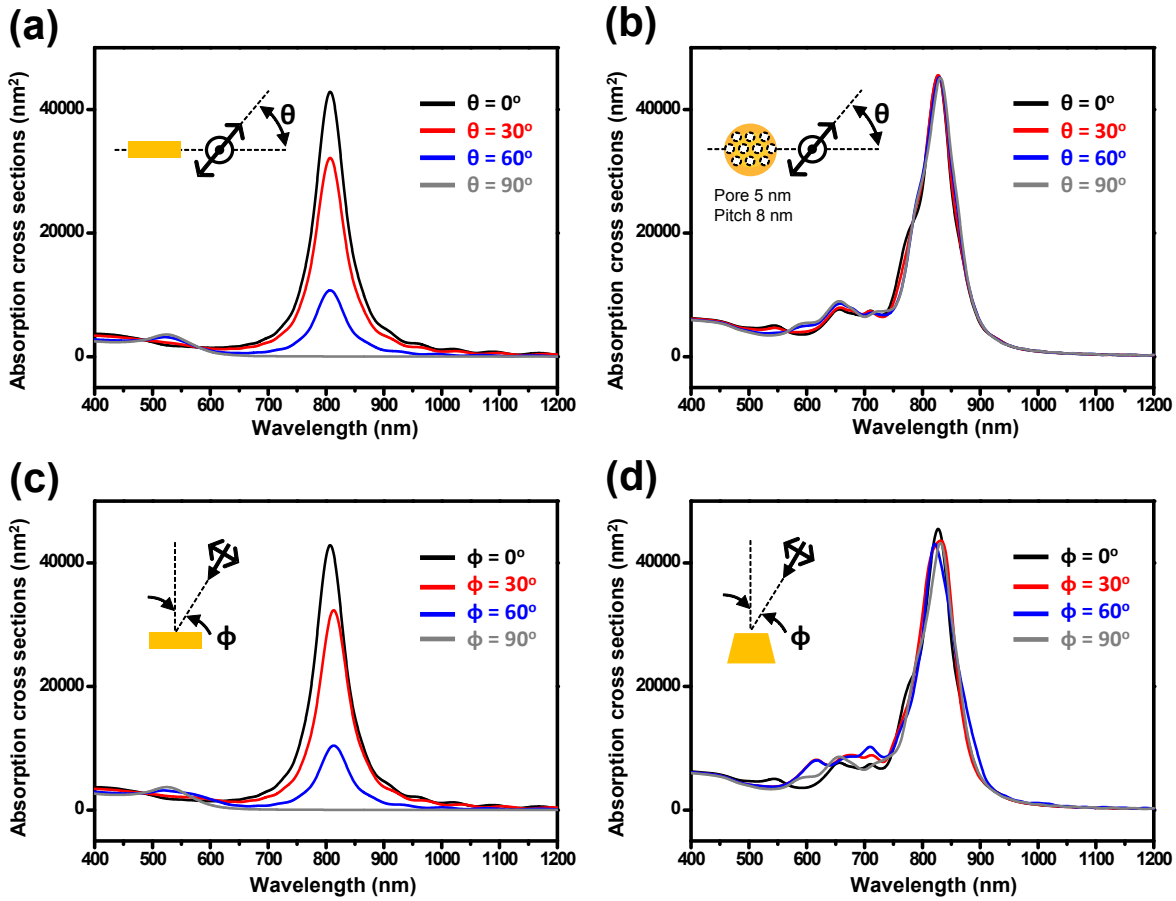

Fig. S5. Calculated absorption cross sections of (a,c) GNRs and (b,d) PGNs. Black, red, blue, and gray graphs indicate the extinction cross sections calculated for four different conditions, as illustrated in the inset figures. The four different (a,b) light polarization angles and (c,d) incident light directions are noted in the graphs. The exterior shape and size of the PGN were the same as those described in Figure 3c. The diameter and the length of the GNR were 25 nm and 90 nm, respectively. The refractive index of the medium was assumed to be 1.33.

6. Estimation of the surface areas of the GNR, the NGN, and the PGN

Based on the microscopic images of the GNRs and the NGNs, the surface areas of the GNR (diameter 25 nm, length 90 nm) and the NGN (upper diameter 50 nm, lower diameter 100 nm, height 50 nm) were calculated as ~8.1×10^3 nm^2 and ~2.3×10^4 nm^2, respectively. Therefore, the surface area of the NGN is already about 3 times larger than that of the GNR. Considering the enlargement of the surface area by a factor of 4~6 from non-porous gold to porous gold,[8,9] the surface area of the PGN could be estimated to be about 15 times larger than that of the GNR.

References

1. C. Earhart, W. Hu, R. Wilson, S. Wang, *Digests of the 5th International Conference on Nanoimprint and Nanoprint Technology, San Francisco*, 2006, 115.
2. J.-S. Wi, S. Sengupta, R. J. Wilson, M. Zhang, M. Tang, S. X. Wang, *Small*, 2011, **7**, 3276-3280.
3. L. Qian, M. Chen, *Appl. Phys. Lett.*, 2007, **91**, 083105.
4. B. Rao, L. Li, K. Maslov, L. Wang, *Opt. Lett.*, 2010, **35**, 1521-1523.
5. S.-W. Lee, H. Kang, J. H. Park, T. G. Lee, E. S. Lee, J. Y. Lee, *J. Opt. Soc. Korea*, 2015, **19**, 55-62.
6. http://www.nanopartz.com/bare_gold_nanorods.asp
7. http://www.bbisolutions.com/molar-concentration-of-nanoparticles
8. F. Zhao, J. Zeng, M. M. P. Arnob, P. Sun, J. Qi, P. Motwani, M. Gheewala, C.-H. Li, A. Paterson, U. Strych, B. Raja, R. C. Wilson, J. C. Wolfe, T. R. Lee and W.-C. Shih, *Nanoscale*, 2014, **6**, 8199-8207.
9. E. Seker, Y. Berdichevsky, M. R. Begley, M. L. Reed, K. J. Staley and M. L. Yarmush, *Nanotechnology*, 2010, **21**, 125504.